Polymer 53 (2012) 801–809

Contents lists available at SciVerse ScienceDirect

Polymer

journal homepage: www.elsevier.com/locate/polymer

Magnetoresistive polyaniline-magnetite nanocomposites with negative dielectrical properties

Hongbo Gu [a,b], Yudong Huang [a,**], Xi Zhang [b], Qiang Wang [d], Jiahua Zhu [b], Lu Shao [a], Neel Haldolaarachchige [e], David P. Young [e], Suying Wei [c,**], Zhanhu Guo [b,*]

[a] School of Chemical Engineering and Technology, Harbin Institute of Technology, Harbin, Heilongjiang 150001, China
[b] Integrated Composites Lab (ICL), Dan F. Smith Department of Chemical Engineering, Lamar University, Beaumont, TX 77710, USA
[c] Department of Chemistry and Biochemistry, Lamar University, Beaumont, TX 77710, USA
[d] Department of Chemistry, University of Oxford, Mansfield Road, Oxford OX1 3TA, United Kingdom
[e] Department of Physics and Astronomy, Louisiana State University, Baton Rouge, LA 70803, USA

ARTICLE INFO

Article history:
Received 21 November 2011
Received in revised form
13 December 2011
Accepted 17 December 2011
Available online 22 December 2011

Keywords:
Magnetic polyaniline nanocomposites
Magnetoresistance
Dielectrical properties

ABSTRACT

Magnetic polyaniline (PANI) polymer nanocomposites (PNCs) reinforced with magnetite (Fe_3O_4) nanoparticles (NPs) have been successfully synthesized using a facile surface initiated polymerization (SIP) method. The chemical structures of the PANI/Fe_3O_4 PNCs are characterized by Fourier transform infrared (FT-IR) spectroscopy. The thermal stability of the PANI/Fe_3O_4 PNCs is performed by thermogravimetric analysis (TGA). Both transmission electron microscopy (TEM) and scanning electron microscopy (SEM) are used to characterize the morphologies of the PANI, Fe_3O_4 nanoparticles (NPs) and the PNCs. X-ray diffraction (XRD) shows a significant effect of the Fe_3O_4 NPs on the crystallization structure of the formed PANI. The dielectrical properties of these PNCs are strongly related to the Fe_3O_4 nanoparticle loadings and unique negative permittivity is observed in all the samples. Temperature dependent resistivity analysis from 50 to 290 K reveals a quasi 3-dimension variable range hopping (VRH) electron conduction mechanism for the nanocomposite samples. The PNCs do not show hysteresis loop with zero coercivity, indicating the superparamagnetic behavior at room temperature. The PNCs with 30 wt% Fe_3O_4 NP loading exhibit a larger positive magnetoresistance (MR = 95%) than 53% of the pure PANI.

1. Introduction

Since the remarkable discovery of the electrical conduction in polymers in 1977 with a publication describing the doping of polyacetylene [1], the conjugated conductive polymers have been developed into a new stage with various applications [2–4]. A significant progress in this field has been made by integrating the unique properties of the conductive polymers with those of various nanoparticles (NPs) in the last two decades [5–8]. Conductive polymer nanocomposites (PNCs) are required for certain applications such as telecoms, electronics [9], fire retardants [10], biosensors [11,12], electrodes for electrodeposition, electrocatalysts for fuel cells [13] and aerospace industry [6] because of their homogeneity, relatively easy processability, and tunable physicochemical properties [14–18]. Consequently, a great variety of PNCs has been synthesized by using the advanced technologies, such as solution blending [19], melt blending [20], layer-by-layer deposition [21], in-situ polymerization [22], electropolymerization [23] and surface initiated polymerization (SIP) [24,25]. However, they still can not meet the desire for devices miniaturization and light weight materials requiring the multifunctional properties [17].

Magnetic NPs [26] including iron, cobalt, nickel and their alloys among them or with others, have captured the intense attention owing to their unique catalytic, magnetic and electrical properties and their wide applications in different areas including catalysis [27], biomedicine [28], magnetic data storage [29] and environmental remediation [30]. Compared with other magnetic NPs, magnetite (Fe_3O_4) is the strongest magnetic NPs of all natural minerals on Earth [31]. Magnetite is a mixed iron oxide with the spinel structure, AB_2O_4, in which the A site is occupied by Fe^{3+} and the B sites have the equal mix of Fe^{3+} and Fe^{2+} [32,33]. It not only has the excellent magnetic properties, but also the admirable conductive properties for the applications in telecommunications

* Corresponding author. Tel.: +1 409 880 7654.
** Corresponding authors.
E-mail addresses: ydhuang.hit1@yahoo.com.cn (Y. Huang), suying.wei@lamar.edu (S. Wei), zhanhu.guo@lamar.edu (Z. Guo).

0032-3861/$ – see front matter © 2011 Elsevier Ltd. All rights reserved.
doi:10.1016/j.polymer.2011.12.033

and sorbents for the adsorption removal of the hazardous heavy metals [34].

Polyaniline (PANI) is one of the most studied conductive polymers due to its easy synthesis, environmental stability, simple doping/dedoping and high conductivity [35,36]. PANI combined with different NPs to form the nanocomposites has great potential applications such as radar-absorber [2], indicators [37], electrochemical capacitors [38], bioelectronic components [39], catalysts [40], gas separation membrane [41], corrosion inhibitor [42], antistatic [43] and semiconductors [8]. Deng et al. [44] have prepared the Fe_3O_4-polyaniline hybrids with coreshell structure in the presence of Fe_3O_4 magnetic fluid in aqueous solution containing dodecylbenzene sulfonic acid sodium salt as a surfactant and dopant. Wan et al. [45] have studied a series of polyaniline composites containing Fe_3O_4 NPs by a template-free method in the presence of β-naphthalene sulfonic acid (NSA) as a dopant, while Long et al. [46] have synthesized the PANI/Fe_3O_4 composites using the template-free method. Yang et al. [47] have investigated the microwave absorption property of the PANI/Fe_3O_4 PNCs. Wang et al. [48] have reported the conductive and magnetic oleic acid modified Fe_3O_4/PANI with multi-core/singe shell nanocomposites with in-situ miniemulsion polymerization approach. However, effective coating of PANI on the Fe_3O_4 NPs is still a challenge, since the surfaces of Fe_3O_4 NPs are hydrophilic but polymers are hydrophobic [49]. Zhu et al. have reported the simple chemical process, surface initiated polymerization (SIP) method, to prepare the PANI PNCs and also studied their formation mechanism [50]. The results confirmed that the oxidant and doping acid have physicochemically attached on the particle surface, which is essentially important for initializing the polymerization starting from the surface of NPs and forming a strong interfacial interaction between PANI and NPs.

The giant magnetoresistance (GMR) effect is a quantum mechanics magnetoresistance effect firstly observed in the thin film structural material, which is composed of alternating ferromagnetic and non-magnetic metal layers [51]. GMR was also found in the nonmultilayer granular magnetic system [52]. This effect indicates a significant resistivity change (large than 1%) in response to an applied external magnetic field [53]. Since the first discovery of GMR effect, GMR sensor has been widely used in many commercial applications, such as magnetic storage (hard disc driver) and biological detection [54]. Although the dielectrical and magnetic properties of the fabricated PANI/Fe_3O_4 PNCs have been reported [45,46], the electron conduction and magnetoresistance under an applied magnetic field in the PANI/Fe_3O_4 fabricated using surface initiated polymerization have been rarely reported.

In this work, we report on the fabrication of conductive magnetic PANI/Fe_3O_4 nanocomposites using the surface initiated polymerization (SIP) method. The chemical structures of the PANI/Fe_3O_4 nanocomposites are characterized by Fourier transform infrared (FT-IR) spectroscopy. The thermal stability of the PANI/Fe_3O_4 nanocomposites is performed by thermogravimetric analysis (TGA). Both transmission electron microscopy (TEM) and scanning electron microscope (SEM) are used to characterize the dispersion of Fe_3O_4 NPs and the morphology of the PANI/Fe_3O_4 nanocomposites. The effects of the Fe_3O_4 NPs on the crystallization structures of the PANI are also studied. The temperature dependent resistivity, frequency dependent permittivity, magnetic properties and magnetroresistance are systematically investigated. The electron conduction mechanism is investigated by the temperature dependent conductivity analysis. The MR behavior is also analyzed based on the current electron-hole (e–h) recombination theory.

2. Experimental

2.1. Materials

Aniline (C_6H_7N), ammonium persulfate (APS, $(NH_4)_2S_2O_8$), and p-toluene sulfonic acid (PTSA, $C_7H_8O_3S$) are purchased from Sigma Aldrich. The Fe_3O_4 NPs are obtained from Nanjing Emperor Nano Material Co., Ltd., China. All the chemicals are used as-received without any further treatment.

2.2. Fabrication of PANI/Fe_3O_4 nanocomposites

PANI/Fe_3O_4 nanocomposites were fabricated with a surface initialized polymerization method. First, the Fe_3O_4 NPs were dispersed in 200 mL deionized water by 2-h sonication. Then PTSA and APS with a fixed ratio of 30 mmol: 18 mmol were added into the above solution followed by 1-h mechanical stirring in an ice-water bath. The aniline solution (36 mmol in 50 mL deionized water, molar ratio of APS:PTSA:Aniline = 3:5:6) was mixed with the above Fe_3O_4 nanoparticle suspension and mechanically stirred continuously for additional 8 h in an ice-water bath for further polymerization. The product was vacuum filtered and washed with deionized water. The precipitant was further washed with methanol to remove any possible oligomers. The final green-black PANI/Fe_3O_4 nanocomposite powders were dried at 50 °C in an oven overnight. The PANI/Fe_3O_4 PNCs with a particle loading of 4.76, 9.09, 16.67 and 30 wt% were fabricated. The pure PANI was fabricated following the above procedures without adding any NPs for comparison.

2.3. Characterizations

The Fourier transform infrared (FT-IR) spectra of the products were obtained on a Bruker Inc. Vector 22 (coupled with an ATR accessory) in the range of 500–4000 cm^{-1} at a resolution of 4 cm^{-1}. X-ray diffraction (XRD) was measured by D/max-rB wide-angle X-ray diffractometer at a Cu k_α wavelength of 0.154 nm. The scanning rate is 4° min^{-1} from 10 to 40°. The scanning electron microscope (SEM) was performed on an FEI Quanta 200F system. The samples are prepared by adhering the powders onto an Al plate. TGA analysis was conducted by TA instruments TGA Q-500 with a heating rate of 10 °C min^{-1} under an air-flow rate of 60 mL min^{-1} from 25 to 700 °C.

Dielectrical properties were investigated by a LCR meter (Agilent, E4980A) equipped with a dielectric test fixture (Agilent, 16451B) at the frequency of 20 Hz to 2 MHz at room temperature. Pure PANI and its PNC powders were pressed in a form of disc pellet with a diameter of 25 mm by applying a pressure of 50 MPa in a hydraulic presser and the average thickness was about 1.0 mm. The same sample was used to measure the resistivity (ρ) by a standard four-probe method from 50 to 290 K. The temperature dependent resistivity was used to determine the electron transport mechanism in pure PANI and its PNCs.

The magnetic properties were investigated in a 9-T Physical Properties Measurement System (PPMS) by Quantum Design. Magnetoresistance was carried out using a standard four-probe technique.

3. Results and discussion

3.1. FT-IR analysis

Fig. 1 shows the FT-IR spectra of the as-received Fe_3O_4 nanoparticles, pure PANI and its nanocomposites reinforced with different nanoparticle loadings. The strong absorption peaks at

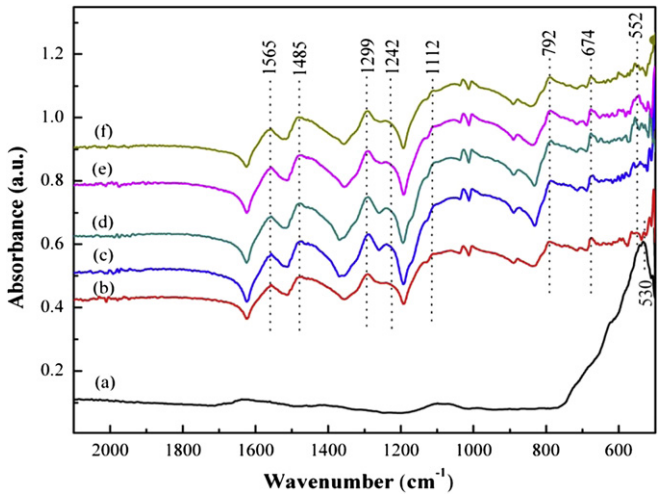

Fig. 1. FT-IR spectra of (a) Fe_3O_4 NPs, (b) pure PANI, and nanocomposites with a nanoparticle loading of (c) 4.76, (d) 9.09 (e) 16.67 and (f) 30 wt%, respectively.

1565 and 1485 cm^{-1} for the pure PANI, Fig. 1(b), correspond to the C=C stretching vibration of the quinoid and benzenoid rings, respectively [55]. The band at 1625 cm^{-1}, with a shoulder at ~1630 cm^{-1}, corresponds to the C=C stretching vibration in a phenazine-like segment [56], which indicates the formation of the quinone form of polymer during the polymerization [57]. The peak at 1299 cm^{-1} is related to the C-N stretching vibration of the benzenoid unit. The peaks at 1242 and 1112 cm^{-1} are assigned to the C-H and C-N stretching vibration of the quinoid rings, respectively. The peak at 674 cm^{-1} is due to the out-of-plane C-H vibration [50,58,59]. The peak at around 792 cm^{-1} is attributed to the out-of-plane bending of C-H in the substituted benzenoid ring. The FT-IR spectra of the PANI/Fe_3O_4 PNCs, Fig. 1(c–f), are almost the same as that of pure PANI. The absorption peak at around 550 cm^{-1} is attributed to the vibration of Fe-O band in Fe_3O_4 nanoparticles, Fig. 1(a), and has a peak shift from 530 cm^{-1} (in the pure Fe_3O_4 nanoparticles) [59] to 552 cm^{-1} (in the PANI/Fe_3O_4 PNCs). This result indicates that the PANI/Fe_3O_4 nanocomposites have been successful synthesized and the observed shift indicates the interaction between PANI and NPs.

3.2. X-ray diffraction analysis

Fig. 2 shows the X-ray diffraction (XRD) patterns of pure PANI and its PANI/Fe_3O_4 PNCs reinforced with different nanoparticle loadings. The diffraction peaks at 2θ = 30.2, 35.6, 43.3, 53.5, and 57.2°, Fig. 2(f), correspond to (220), (311), (400), (422) and (511) crystallographic planes of the spinel phase of Fe_3O_4, respectively [60,61]. The average crystallite size can be estimated by XRD pattern, using the Scherrer Equation (1) [62]:

$$\beta = \frac{k\lambda}{L\cos\theta} \quad (1)$$

where λ is the X-ray wavelength (λ = 0.154 nm), L is the average crystallite size, k is the shape factor, β is the full-width at half-maximum, and θ is Bragg angle in degree. The shape factor k, depending on several factors, including the miller index of the reflection plane and the shape of the crystal, is normally 0.89. The peak at 2θ = 35.6° is chosen to calculate the crystallite size, the average crystallite size of the Fe_3O_4 NPs is about 12.8 nm. Similar results are obtained in the nanocomposites, which is about 13.4 nm. The two broad peaks at 2θ = 20.2 and 25.2°, Fig. 2(a), correspond to the (100) and (110) crystallographic planes of the partially

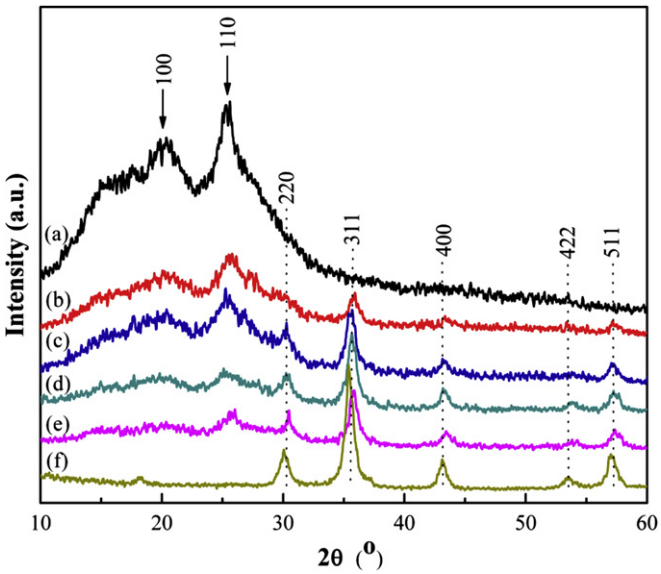

Fig. 2. The XRD patterns of (a) pure PANI, and the nanocomposites with a nanoparticle loading of (b) 4.76, (c) 9.09 (d) 16.67 and (e) 30 wt%, and (f) pure Fe_3O_4 NPs.

crystalline PANI [63,64]. Obviously, the diffraction peaks of the Fe_3O_4 NPs appear in the PANI/Fe_3O_4 nanocomposites, Fig. 2(b–e) and the intensity of these peaks becomes stronger with increasing the nanoparticle loadings, while the two original peaks of PANI show a reduced intensity at 2θ = 20.2 and 25.2°. This indicates a strong effect of the Fe_3O_4 NPs on the crystallization structures of the formed PANI and the interaction between PANI backbone and Fe_3O_4 NPs [65]. This result indicates that PANI has been successfully anchored on the surface of Fe_3O_4 NPs through the SIP method.

3.3. Thermogravimetric analysis

Fig. 3 shows the TGA curves of pure PANI and its Fe_3O_4 PNCs in the air. Two-stage weight losses are observed in all the samples. The first stage in the temperature range from room temperature to 250 °C is attributed to the elimination of moisture and dopant anions in the samples. The major weight loss of all the samples from 300 to 600 °C is due to a large scale thermal degradation of the PANI chains [49,66,67]. The terminal degradation temperature of the PANI is 629 °C, with no residue remaining under the

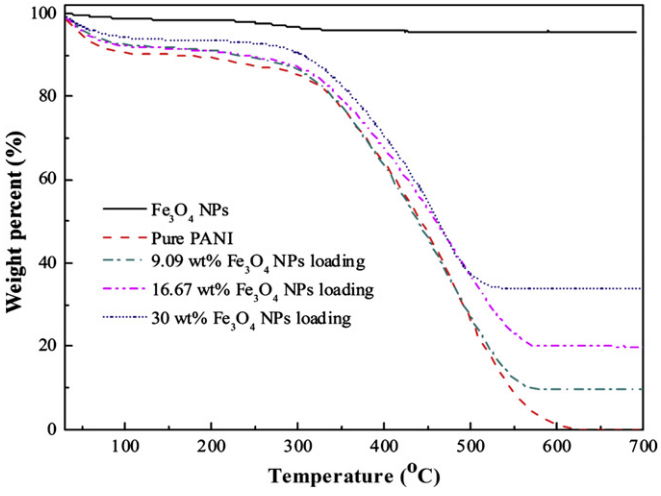

Fig. 3. The TGA curves of pure PANI, its Fe_3O_4 nanocomposites and pure Fe_3O_4.

experiment conditions. The TGA curves of the PANI/Fe_3O_4 PNCs with different nanoparticle loadings are observed to be very similar to that of the PANI, Fig. 3. However, the weight residues of the PNCs with an initial nanoparticle loading of 9.09, 16.67 and 30 wt% are 9.71, 19.96 and 33.05%, respectively. The weight difference is due to the incomplete polymerization of the monomers. The 15 wt% loss decomposition temperature for pure PANI and the PNCs with a particle loading of 9.09, 16.67, 30 wt% are 303, 312, 319 and 338 °C, respectively. This result indicates that the thermal stability of PANI/Fe_3O_4 PNCs is improved with the addition of Fe_3O_4 NPs.

3.4. Microstructures of the nanocomposites

The SEM and TEM images of the Fe_3O_4 NPs, pure PANI and PANI/Fe_3O_4 nanocomposites are shown in Figs. 4 and 5, respectively. Fig. 4(a) shows that the Fe_3O_4 nanoparticles are ball-like with a diameter of 80–100 nm. However, the TEM image illustrates that these balls are composed of some smaller particles with an average diameter of 12 nm, Fig. 5(a), which is consistent with the results obtained from XRD. This indicates that some of the Fe_3O_4 NPs agglomerate due to the magneto-dipole interactions between NPs [44]. Compared with pure PANI, Figs. 4b and 5b, the Fe_3O_4 NPs have been well-coated with PANI in the nanocomposites, Figs. 4c and 5c. The surface of the PNCs becomes rougher, which is due to the polymerization occurred on the surface of NPs and the strong interfacial interaction between the polymer matrix and NPs [50]. In the nanocomposites, the Fe_3O_4 NPs are observed to be fairly well dispersed in the PANI matrix and some agglomerated NPs are also observed in the PNCs, Fig. 5(c).

3.5. Dielectrical properties

Dielectrical properties describe the ability that an electrical medium can be polarized by an applied electric field [68]. When a dielectric medium is placed in an electric field, electrical charges shift from their average equilibrium positions causing dielectric polarization. The frequency dependence reflects a fact that the polarization of these materials does not respond to an applied electric field instantaneously. Thus, the permittivity is often described as a complex permittivity $\varepsilon^*(\omega)$ ($\omega = 2\pi f$, f is the measuring frequency) [69]:

$$\varepsilon^*(\omega) = \frac{D_0}{E_0}(\cos\omega\tau - j\sin\omega\tau) \tag{2}$$

where, D_0 and E_0 are the amplitudes of the electric displacement and electrical fields, respectively; τ is the relaxation time (which is required when the electric field is removed and the materials return to the original state). At very low frequency ($\omega << 1/\tau$), dipoles follow the change of the field and the value of $\varepsilon^* \approx \varepsilon_s$, where ε_s is the permittivity at low frequency limit, also called the static permittivity. At the very high frequency ($\omega >> 1/\tau$), dipoles can no longer follow the change of the electric field any more and the value of $\varepsilon^* \approx \varepsilon_\infty$, where ε_∞ is the permittivity at high frequency limit. So the complex form of the permittivity is [70]:

$$\varepsilon^*(\omega) = \varepsilon'(\omega) - j\varepsilon''(\omega) = \varepsilon_s + \frac{(\varepsilon_s - \varepsilon_\infty)}{1 + j\omega\tau} \tag{3}$$

where, ε' is the real part of the ε^*, it represents the energy storage within the medium; ε'' is the imaginary part of the ε^*, it stands for the dissipation (or loss) of the energy within the medium. And when the frequency reaches the characteristic frequency ($\omega = 1/\tau$), the dielectric constant changes dramatically.

The conductive PANI in a metallic state has remarkable frequency dependent conductivity, which means that the dielectic

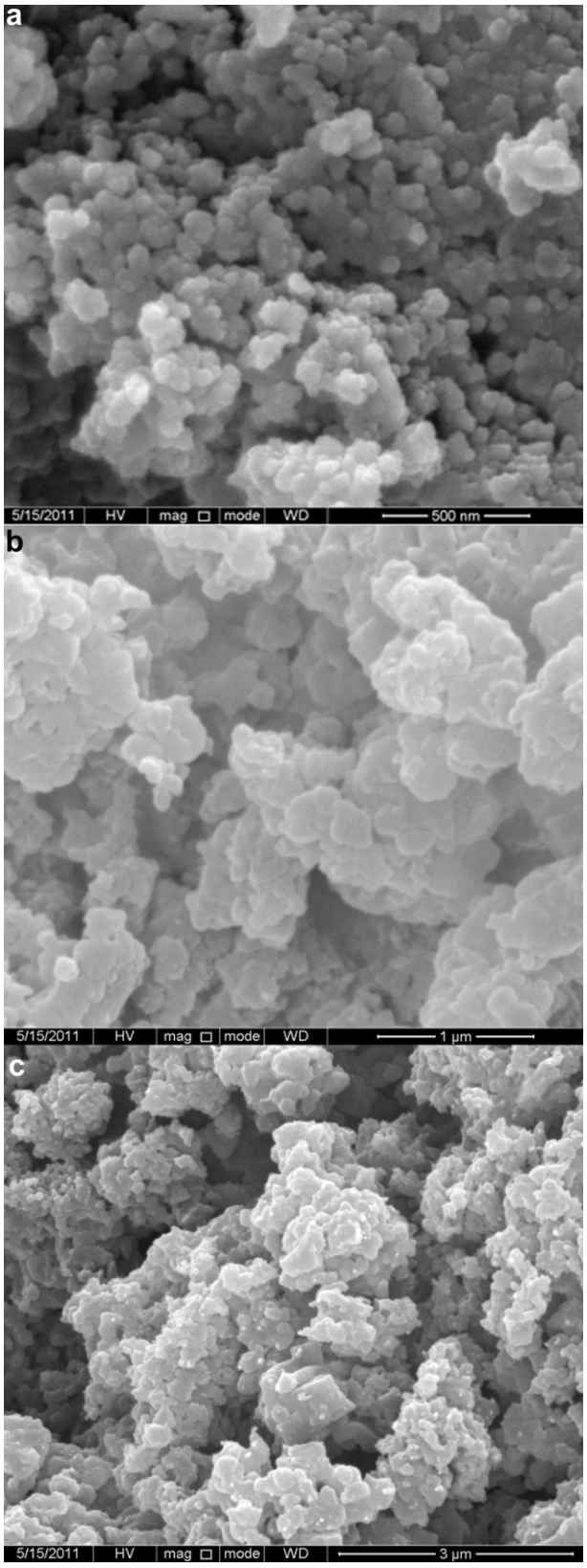

Fig. 4. SEM images of (a) Fe_3O_4 NPs, (b) pure PANI, and (c) PNCs with 4.76 wt% Fe_3O_4 nanoparticle loading.

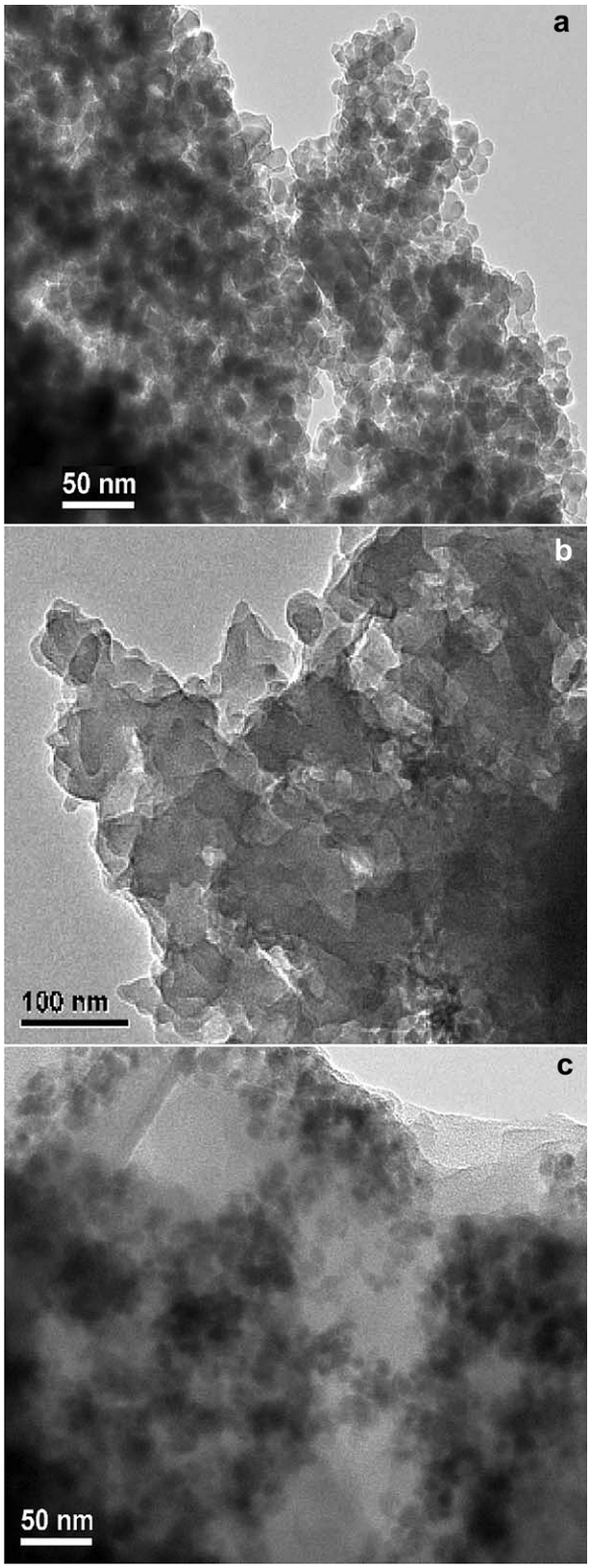

Fig. 5. TEM images of (a) Fe_3O_4 NPs, (b) pure PANI, and (c) PNCs with 4.76 wt% Fe_3O_4 nanoparticle loading.

property has a strong effect on the conductivity of polyaniline [71]. The interchain interaction for polyaniline is an important factor affecting its conductivity (σ) [72]. Even though the σ can be improved with an increase in the crystallinity, the conductive PANI remains considerably disordered. In the conductive polymer composites, the transport of free charge carriers becomes more complicated when the systems become more disordered [73]. However, in the crystalline regions, including regions of well-ordered polymer chains (called metallic island), the interchain interaction is sufficiently strong to allow the charge carriers to be delocalized among the crystalline regions, i.e., within the disordered regions [74]. Each metallic island in the polymers represents crystalline domains with the delocalized electrons embedded in the amorphous PANI. Fig. 6 depicts the real permittivity (ε') and imaginary permittivity (ε'') and dielectric loss tangent (tan δ, where tan $\delta = \varepsilon''/\varepsilon'$) as a function of the frequency for pure PANI and its nanocomposites with different nanoparticle loadings at room temperature. In Fig. 6(a), ε' at frequency lower than 10^5 Hz increases with increasing the frequency due to the space charge polarization [75] and after that ε' reaches the equilibrium maximum and then never goes up. A high positive ε' means that the mobile charges are no longer free and localized in each metallic island. The charges could not hop to the vicinity of the metallic regions, but rather remain confined to the domain of the metallic island. However, a negative ε' represents the charge delocalization in a macroscopic scale, indicating an intrinsic metallic state [74]. All the samples prepared using SIP method show a negative permittivity within the whole frequency range at room temperature, which means that they have a weak localization behavior and the intrinsic metallic nature of the PANI. The PANI/Fe_3O_4 nanocomposites containing 16.67 wt% of the Fe_3O_4 NPs have the lowest negative ε' due to the fact that its Fe_3O_4 NPs proportion reached the percolation threshold, providing the highest level of charge delocalization for the PANI [76]. Adding more Fe_3O_4 NPs interrupts the charge transport and limits the charge delocalization. Similar to the value of ε', tan δ curves are shown in Fig. 6(c), which exhibits the most stable and lowest dielectric loss at around -0.15 after 10^6 Hz. The value of ε'' significantly decreases within the frequency range from 10^3 to 10^5 Hz and thereafter is almost stable, Fig. 6(b). The PANI/Fe_3O_4 nanocomposites containing 16.67 wt% Fe_3O_4 NPs obtain the highest ε'' and lowest dielectric loss compared with other samples.

3.6. Temperature dependent resistivity - electron transport mechanism

The temperature dependent resistivity of pure PANI and its nanocomposites with different Fe_3O_4 loadings is measured at temperatures ranging from 50 to 290 K to determine the electron transport mechanism, Fig. 7(a and b). Generally, the resistivity of all the samples decreases with increasing temperature, exhibiting a typical semiconductor behavior in the measured temperature scale [77], Fig. 7(a). The decrease in resistivity with the addition of Fe_3O_4 NPs and the slight difference in resistivity (from 1.16×10^2 to 2.64×10^2 Ω cm) are observed in the PNCs with a nanoparticle loading of 4.76–16.67 wt%, thereafter the resistivity of the PNCs with a nanoparticle loading of 30 wt% dramatically increases (about 1.27×10^3 Ω.cm). On one hand, in the disordered systems, two aspects of the conductivity, i.e., microscopic conductivity and macroscopic conductivity, have been studied for the multifunctional materials [78]. Microscopic conductivity does not have much difference due to the same preparation conditions. However, the macroscopic conductivity is often varied because of the compactness and molecular orientation, depending on the aniline content in the nanocomposites. The decreased resistivity can be attributed

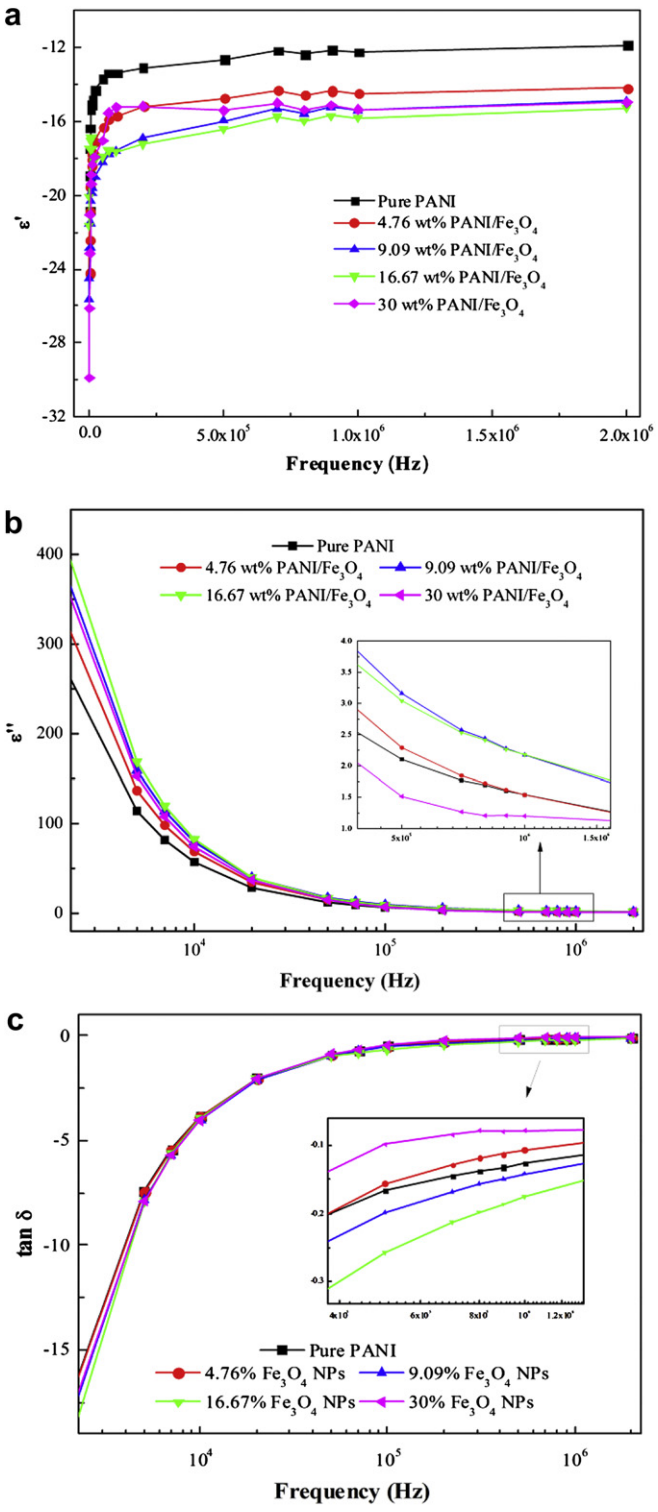

Fig. 6. (a) Real permittivity, (b) Imaginary permittivity and (c) Dielectric loss tangent as a function of frequency for pure PANI and its PNCs with different nanoparticle loadings.

to the increased compactness arising from the presence of the Fe_3O_4 NPs during the growth of the PANI chains [77]. When the compactness achieves the maximum threshold of the Fe_3O_4 nanoparticle content, the further increasing of the Fe_3O_4 nanoparticles affects the growth of PANI and decreases the compactness of the materials, which thereby causes an increased resistivity. On the other hand, the conductivity of PANI is strongly dependent on

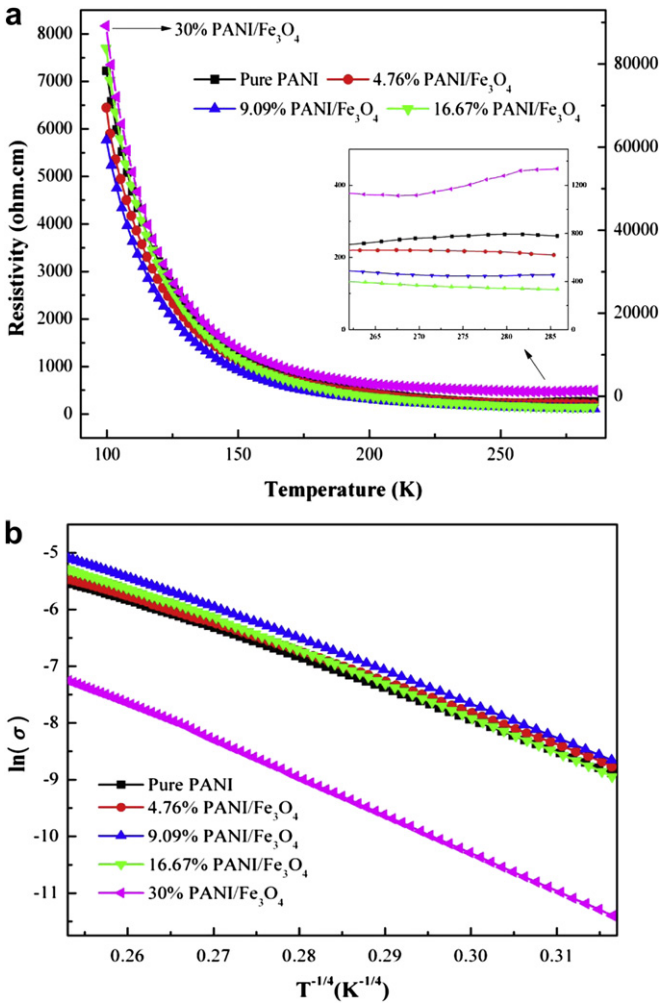

Fig. 7. (a) Resistivity vs. temperature, and (b) ln (σ) ~ $T^{-1/4}$ curves of pure PANI and its nanocomposites with different nanoparticle loadings.

the doping acid (dopant) with electron donor ability [79–81]. The addition of the Fe_3O_4 NPs affects the interaction between the PANI polymer matrix and the doping acid, decreases the doping degree [62] and partially hinders the electron transport pathway. The resistivity of the PANI/Fe_3O_4 PNCs (the content of Fe_3O_4 is 9.12 wt%) by Deng et al. [40] using an in-situ polymerization has been reported 6.54×10^2 Ω cm, which is higher than 4.46×10^2 Ω cm of SIP method, and the resistivity of PANI/Fe_3O_4 PNCs (the content of Fe_3O_4 is 20 wt%) by Zhang et al. [44,45] using a self-assembly method is about 93.5 Ω cm, which is slightly lower than 1.16×10^2 Ω cm of SIP method.

The electron transport mechanism is investigated by Mott variable range hopping (also called VRH) approach [82,83], which is a model depicting the low temperature conduction in strongly disordered systems with localized states. VRH is presented in Equation (4) [50]:

$$\sigma = \sigma_0 \exp\left[-\left(\frac{T_0}{T}\right)^{1/n+1}\right], \quad n = 1, 2, 3 \tag{4}$$

where, the pre-exponential factor σ_0 is a constant, which represents the conductivity at high temperature limit, T_0 is the hopping barrier, which stands for the characteristic Mott temperature, the energy needed for charge carrier's hopping conduction and T is the Kelvin temperature. The n value of 4, 3, and 2 is for three-, two-, and one- dimensional systems, respectively. σ_0 and T_0 can be calculated

by the plot ln (σ) ~ $T^{-1/n+1}$. The temperature dependent resistivity follows ln (σ) ~ $T^{-1/4}$ linear relationship, Fig. 8(b), which indicates a quasi 3-dementional VRH hopping mechanism in pure PANI and its PANI/Fe_3O_4 nanocomposites. The σ_0 and T_0 obtained from Fig. 8(b) are summarized in Table 1. Both σ_0 and T_0 increase with increasing nanoparticle loadings, except in the PNCs with a 4.76 wt % Fe_3O_4 nanoparticle loading. Generally, the parameter T_0 is inversely proportional to the localization length of the charge carriers [84], which means the larger T_0, the stronger charge carrier scattering, and the more increased resistivity. However, it's interesting to see that the bigger T_0 corresponds to the higher σ_0, which is due to the modulated electromagnetic wave in the nanostructures of these nanocomposites. This is consistent with our previous research observations in the polyaniline-tungsten oxide nanocomposites [55].

3.7. Magnetic properties

Magnetization is a phenomenon describing how the magnetic materials react to an applied external magnetic field. Application of a magnetic field could align the magnetic moment of the nanoparticles in the field direction, and then the magnetization rises until it reaches the saturation magnetization (M_s) with increasing field [78]. When the diameter of the magnetic NPs is around 10 nm, depending on the materials, the coercive force (H_c, which is an important physical parameter to distinguish a material whether it is hard (>100 Oe) or soft (<100 Oe)) will decrease to zero and then the NPs will be in the superparamagnetic state [85]. This only occurs in soft magnetic materials in a magnetic field. The magnetic properties of a superparamagnetic system can be described on the basis of the Langevin Equation [85]:

$$M/M_s = \coth x - 1/x \quad (5)$$

where, M is magnetization (emu g^{-1}) in magnetic field H (Oe), M_s is saturation magnetization and $x = aH$. The parameter a is related to the electron spin magnetic moment m (J T^{-1} or μ_B, μ_B is the Bohr magneton) of the individual molecule:

$$a = m/kT \quad (6)$$

where, k is the Boltzman constant, and T is the absolute temperature.

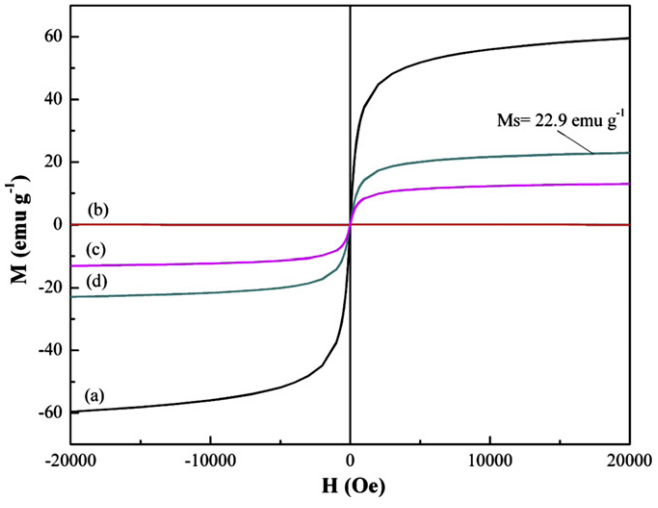

Fig. 8. Room temperature magnetic hysteresis loops of (a) pure Fe_3O_4 NPs, (b) pure PANI and PANI/Fe_3O_4 PNCs with of a nanoparticle loading of (c) 9.09 and (d) 30 wt%.

Table 1
T_0 and σ_0 for pure PANI and its nanocomposites.

Samples	$T_0 \times 10^7$ (K)	σ_0 (S cm^{-1})
Pure PANI	0.70	1826
4.76 wt% Fe_3O_4 NPs	0.64	1437
9.09 wt% Fe_3O_4 NPs	0.93	7531
16.67 wt% Fe_3O_4 NPs	1.01	8325
30 wt% Fe_3O_4 NPs	1.79	10302

Fig. 8 shows the magnetization curves of the as-received Fe_3O_4 NPs, pure PANI and its nanocomposites reinforced with a nanoparticle loading of 9.09 and 30 wt% at $T = 290$ K. The pure PANI polymer is observed to be non-magnetic as expected, whereas the curves of the others show no hysteresis loops, in which the coercivity approaches zero Oe, exhibiting a superparamagnetic behavior [86]. The M_s of the as-received Fe_3O_4 NPs is not reached even at high magnetic field and is determined by the extrapolated saturation magnetization obtained from the intercept of $M \sim H^{-1}$ at high field [18,87]. The calculated M_s of the as-received Fe_3O_4 NPs is 57.38 emu g^{-1}, which is smaller than the bulk Fe_3O_4 (92–100 emu g^{-1}) [88]. The M_s values of the PNCs with nanoparticle loadings of 9.09 and 30 wt% after dispersion in the polyaniline matrix are observed to be saturated at a lower field and are about 5.0 and 22.9 emu g^{-1}, respectively. The particle loadings for 9.09 and 30 wt% estimated from the M_s are found to be 8.89 and 39.91 wt%, which is consistent with the results obtained from TGA. The PANI/Fe_3O_4 nanocomposites with a nanoparticle loading of 30 wt% exhibit the largest magnetization among the nanocomposites.

The nonlinear fitting of magnetization (M) and magnetic field (H) using Polymath software is applied to obtain the best fit to Equation (5). The values of M_s for the pure Fe_3O_4 NPs and the PNCs with nanoparticle loadings of 9.09 and 30 wt%, determined from the fit, are 56.916, 4.983 and 22.081 emu g^{-1}, respectively. However, the parameter a for the pure Fe_3O_4 and different nanoparticle loadings is almost the same with a value of 3.35×10^{-3} T^{-1} and the fitting correlation coefficient R^2 is 0.9983. The magnetic moment m can be calculated from a according to the Equation (6) and the value is 1.34×10^{-23} J T^{-1} (about $1.44\mu_B$), which is below the bulk magnetic moment of Fe_3O_4 (about 4 μ_B) [89].

3.8. Magnetoresistance

Magnetoresistance (MR), defined as $\Delta R/R = [R(H)-R(0)]/R(0)$, indicates a property of materials to change electrical resistance in response to an external magnetic field, relying on the spin-dependent scattering at the interfaces and spin-polarized carrier transport in the spacer [90]. The charge carrier transport path length increases due to the effect of Lorentz force, when an external field is applied to the materials [91]. In contrast, the amount of the charge carrier along with the electric field direction becomes lower and the resistance increases.

Fig. 9 illustrates the MR of pure PANI and 30 wt% PANI/Fe_3O_4 nanocomposites at 290 K. The MR of the nanocomposites is related to the loading of Fe_3O_4 nanoparticles. All the samples exhibit a positive MR throughout the whole measurement, especially for the 30 wt% PANI/Fe_3O_4 nanocomposites (MR = 95%). A large MR up to ~10% is recorded at room temperature for relative small magnetic fields of $H \sim 100$ Oe, which corresponds to the magnetic length $L_H = 2.5 \times 10^3$ Å (where $L_H = \sqrt{\hbar/eH}$, $\hbar = h/2\pi$, e is the electric charge of electron, h is Planck constant) [91]. And the effect of Lorentz force on the electrons is negligible. For the 30 wt% PANI/Fe_3O_4 nanocomposites, a large anomalous MR is observed (~7.3% at 500 Oe, up to 11% at 1000 Oe, both at room

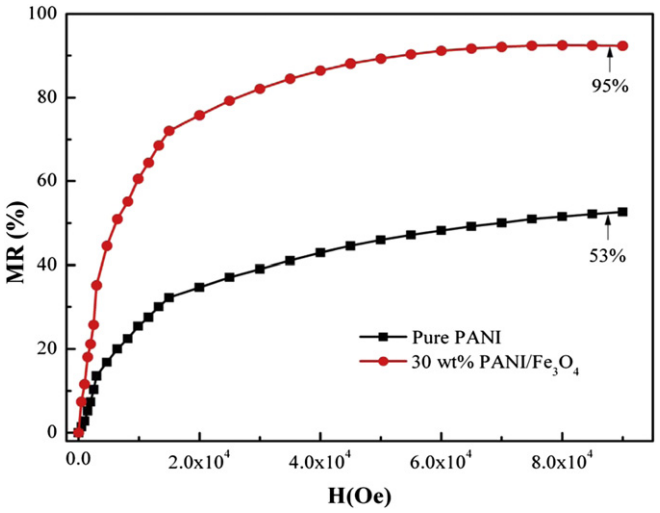

Fig. 9. Magnetoresistance of pure PANI and 30 wt% PANI/Fe_3O_4 nanocomposites at $T = 290$ K.

temperature), which means it has a very high sensitivity to the external applied magnetic field and could be applied as active elements in the electronic devices such as magnetic field sensors [92]. Prigodin et al. [91] have reported the mechanism for this large MR effect to explain the anomalous positive MR in the thin films of organic semiconductor based on the charge transport being electron-hole (e–h) recombination in the chemical reaction with radicals as "chemically induced dynamic spin polarization". They suggest that, of the parameters influencing the electrical current density, J, the e–h recombination rate β is the most sensitive to changes in an applied magnetic field H. Assuming the relative modulation of β (H) and the respective modulation of $J(\beta)$ with magnetic field are small, the expression for MR can be described as following [91]:

$$\mathrm{MR} = \frac{J(0)}{J(H)} - 1 = c\left[1 - \frac{\beta(0)}{\beta(H)}\right] \tag{7-a}$$

$$c = -\left(\frac{\beta}{J(\beta)}\right)\frac{\mathrm{d}J}{\mathrm{d}\beta} = -\frac{\mathrm{dln}J}{\mathrm{dln}\beta}\Big|H = 0 \tag{7-b}$$

where, the factor c is dependent on β. For the space charge limited transport, Parmenter and Ruppel have found the exact solution [93]:

$$J = \left(\frac{3}{2}\right)\left[\frac{\pi e \varepsilon_0 \varepsilon_r \mu_p \mu_n \left(\mu_p + \mu_n\right)}{\beta}\right]^{1/2}\left(\frac{V^2}{L^3}\right) \tag{8}$$

where, μ_n and μ_p represent the effective mobilities of the injected electron and holes, respectively. V is the voltage drop across the semiconductor film of thickness L, ε_0 stands for the dielectric constant of vacuum and ε_r the relative dielectric constant of the semiconductor.

They claimed that the e–h recombination process passes through an intermediate state which represents a coupled state of the electron and hole and assumed that b is the corresponding formation rate constant of the e–h pair forms [91]. And the e–h pair may either dissociate or recombine. Using k_s and k_t to describe the rate of recombination, which depends on its spin state, for singlet and triplet e–h pairs, respectively, q_s and q_t represent the rate of dissociation for singlet and triplet state, respectively, the e–h recombination rate β in Equation (7) and Equation (8) could be described as below:

$$\beta = b\left[\left(\frac{1}{4}\right)\frac{k_s}{k_s + q_s} + \left(\frac{3}{4}\right)\frac{k_t}{k_t + q_t}\right] \tag{9}$$

The coefficients for each term in square-brackets of Equation (9) are the relative ratio between singlets and triplets for an uncorrelated distribution of spins for injected electrons and holes. All four spin states are expected to stay equally occupied at any time, so the recombination rate is [91]:

$$\beta(0) = \frac{b(k_s + 3k_t)}{k_s + 3k_t + q_s + 3q_t} \tag{10}$$

For the strong magnetic fields, the e–h recombination is [91]:

$$\beta(\infty) = b\left[\left(\frac{1}{2}\right)\frac{k_s + k_t}{k_s + k_t + q_s + q_t} + \left(\frac{1}{2}\right)\frac{k_t}{k_t + q_t}\right] \tag{11}$$

Substituting Equations (10) and (11) into Equations (7) and (8) and rearranging, the saturation magnetroresistance, $\mathrm{MR_{sat}}$:

$$\mathrm{MR_{sat}} = -\left(\frac{1}{2}\right)\frac{(k_s + q_s - k_t - q_t)(k_s q_t - k_t q_s)}{(k_t + q_t)(k_s + 3k_t + q_s + 3q_t)(k_s + k_t + q_s + q_t)} \tag{12}$$

when $k_s = k_t = k$, Equation (11) is described as following:

$$\mathrm{MR_{sat}} = \left(\frac{1}{2}\right)\frac{k(q_s + q_t)^2}{(k + q_t)(4k + q_s + 3q_t)(2k + q_s + q_t)} \tag{13}$$

The positive MR in Equation (13) illustrates that the recombination rates of the singlet and triplet are equal and the dissociation rates are different. The splitting of the triplet channels by magnetic fields results in a slow e–h recombination. As discussed in the temperature dependent resistivity section, the samples obtained exhibit a typical semiconductor behavior in the measured temperature scale, which means that this theory can also be applied to our PANI/Fe_3O_4 nanocomposite system.

4. Conclusions

Polyaniline nanocomposites reinforced with different Fe_3O_4 nanoparticle loadings have been synthesized using a surface initiated polymerization (SIP) method. The FT-IR and TGA results demonstrated the formation of polyaniline in the presence of the Fe_3O_4 NPs. Both TEM and SEM indicate that the Fe_3O_4 NPs have been well-coated with PANI. XRD shows the significant effects of the Fe_3O_4 NPs on the crystallization behavior of the PANI. The dielectric properties of these PNCs are strongly related to the Fe_3O_4 nanoparticle loading, and the PANI and its nanocomposites show a negative permittivity. Mott variable range hopping (VRH) model is introduced to evaluate the electron transport mechanism of these nanocomposites and the results indicate a quasi 3-dimension VRH conduction mechanism. Pure PANI shows a non-magnetic property and the PNCs do not show hysteresis loop, indicating a superparamagnetic behavior. A large anomalous and positive MR is observed in the polymer and its nanocomposites with 30 wt% Fe_3O_4 nanoparticle loading and interpreted based on the currently available electron-hole (e–h) recombination theories.

Acknowledgment

This project is financially supported by the National Science Foundation Nanoscale Interdisciplinary Research Team, and Materials Processing and Manufacturing (CMMI 10-30755). H. Gu acknowledges the support from Chinese Scholarship Council (CSC) program.

References

[1] Chiang CK, Fincher Jr CR, Park YW, Heeger AJ, Shirakawa H, Louis EJ, et al. Phys Rev Lett 1977;39:1098–101.
[2] Makeiff DA, Huber T. Synth Met 2006;156:497–505.
[3] Sun Z, Zussman E, Yarin AL, Wendorff JH, Greiner A. Adv Mater 2003;15:1929–32.
[4] Forrest SR. Nature 2004;428(6986):911–8.
[5] Chandrakanthi RLN, Careem MA. Thin Solid Films 2002;417:51–6.
[6] Jung YJ, Kar S, Talapatra S, Soldano C, Viswanathan G, Li X, et al. Nano Lett 2006;6(3):413–8.
[7] Sih BC, Wolf MO. Chem Commun 2005;27:3375–84.
[8] Godovsky DY, Varfolomeev AE, Zaretsky DF, Nayana CRL, Kundig A, Weder C, et al. J Mater Chem 2001;11:2465–9.
[9] Wei S, Mavinakuli P, Wang Q, Chen D, Asapu R, Mao Y, et al. J Electrochem Soc 2011;158(11):K205–12.
[10] Kashiwagi T, Du F, Douglas JF, Winey KI, Harris RH, Shields JR. Nat Mater 2005;4:928–33.
[11] Virji S, Kojima R, Fowler JD, Villanueva JG, Kaner RB, Veiller BH. Nano Res 2009;2:135–42.
[12] Feng X, Li R, Ma Y, Fan Q, Huang W. Synth Met 2011;161:1940–5.
[13] Ding K, Jia H, Wei S, Guo Z. Ind Eng Chem Res 2011;50:7077–82.
[14] Zhu J, Wei S, Zhang L, Mao Y, Ryu J, Mavinakuli P, et al. J Phys Chem C 2010;114(39):16335–42.
[15] Corbierre MK, Cameron NS, Sutton M, Mochrie SGJ, Lurio LB, Ruehm A, et al. J Am Chem Soc 2001;123:10411–2.
[16] Yong V, Hahn HT. Nanotechnology 2004;15:1338–43.
[17] Roy CK, Sahoo Y, Prasad PN. Adv Mater 2005;17(23):2877–81.
[18] Guo Z, Henry LL, Palshin V, Podlaha EJ. J Mater Chem 2006;16:1772–7.
[19] Yun SI, Attard D, Lo V, Davis J, Li H, Latella B, et al. J Appl Polym Sci 2008;108:1550–6.
[20] Lin B, Genaro AG, Joel AH, Petra P, Uttandaraman S. Macromol Mater Eng 2008;293:631–40.
[21] Lange U, Ivanov S, Lyutov V, Tsakova V, Mirsky V. J Solid State Electrochem 2010;14:1261–8.
[22] Breuer O, Uttandaraman S. Polym Compos 2004;25:630–45.
[23] Huang L, Wang Z, Wang H, Cheng X, Mitra A, Yan Y. J Mater Chem 2002;12:388–91.
[24] Guo Z, Kim TY, Lei K, Pereira T, Hahn HT. Compos Sci Technol 2008;68:164–70.
[25] Guo Z, Park S, Wei S, Pereira T, Moldovan M, Karki AB, et al. Nanotechnology 2007;18:335704.
[26] Wei S, Wang Q, Zhu J, Sun L, Lin H, Guo Z. Nanoscale 2011;3:4474–502.
[27] Lu AH, Schmidt W, Matoussevitch N, Bönnemann H, Spliethoff B, Tesche B, et al. Angew Chem Int Ed 2004;43:4303–6.
[28] Gupta AK, Gupta M. Biomaterials 2005;26:3995–4021.
[29] Lei Z, Bi S. Mater Lett 2007;61:3531–4.
[30] Zhang D, Wei S, Kaila C, Su X, Wu J, Karki AB, et al. Nanoscale 2010;2:917–9.
[31] Yu H, Chen M, Philip MR, Wang S, White RL, Sun S. Nano Lett 2005;5(2):379–82.
[32] Duffy JA, Taylor JW, Dugdale SB, Shenton TC, Butchers MW, Giblin SR, et al. Phys Rev B 2010;81:134424.
[33] Lima EJ, Brandl AJ, Arelaro AD, Goya GF. J Appl Phys 2006;99:083908.
[34] Mayo JT, Yavuz C, Yean S, Cong L, Shipley H, Yu W, et al. Sci Technol Adv Mater 2007;8:71–5.
[35] Chiang JC, MacDiarmid AG. Synth Met 1986;13:193–205.
[36] Stejskal J, Gilbert RG. Pure Appl Chem 2002;74:857–67.
[37] Drelinkiewicz A, Waksmundzka-Góra A, Sobczak JW, Stejskal J. Appl Catal A 2007;333:219–28.
[38] Sun LJ, Liu XX, Lau KKT, Chen L, Gu WM. Electrochim Acta 2008;53:3036–42.
[39] Willner I, Willner B, Katz E. Bioelectrochemistry 2007;70:2–11.
[40] Amaya T, Nishina Y, Saio D, Hirao T. Chem Lett 2008;37:68–9.
[41] Weng CJ, Jhuo YS, Huang KY, Feng CF, Yeh JM, Wei Y, et al. Macromolecules 2011;44:6067–76.
[42] Berhard W. Adv Mater 1994;6(3):226–8.
[43] Soto-Oviedo MA, Olacir AA, Faez R, Rezende MC, Paoli MAD. Synth Met 2006;156:1249–55.
[44] Deng J, He C, Peng Y, Wang J, Long X, Li P, et al. Synth Met 2003;139:295–301.
[45] Zhang Z, Wan M. Synth Met 2003;132:205–12.
[46] Long Y, Chen Z, Duvail JL, Zhang Z, Wan M. Physica B 2005;370:121–30.
[47] Yang C, Du J, Peng Q, Qiao R, Chen W, Xu C, et al. J Phys Chem B 2009;113:5052–8.
[48] Wang H, Wang R, Wang L, Tian X. Colloids Surf A 2011;384:624–9.
[49] Xuan SH, Wang YXJ, Leung KCF, Shu K. J Phys Chem C 2008;112:18804–9.
[50] Zhu J, Wei S, Zhang L, Mao Y, Ryu J, Haldolaarachige N, et al. J Mater Chem 2011;21:3952–9.
[51] Baibich MN, Broto JM, Fert A, Van Dau FN, Petroff F, Etienne P, et al. Phys Rev Lett 1988;61:2472–5.
[52] Xiao JQ, Jiang JS, Chien CL. Phys Rev Lett 1992;68:3749–52.
[53] Guo Z, Park S, Hahn HT, Wei S, Moldovan M, Karki AB, et al. Appl Phys Lett 2007;90:053111.
[54] Edelstein RL, Tamanaha CR, Sheehan PE, Miller MM, Baselt DR, Whitman LJ, et al. Biosens Bioelectron 2000;14:805–13.
[55] Zhu J, Wei S, Zhang L, Mao Y, Ryu J, Karki AB, et al. J Mater Chem 2011;21:342–8.
[56] Stejskal J, Sapurina I, Trchová M, Konyushenko EN. Macromolecules 2008;41:3530–6.
[57] Murakami Y, Tachi Y, Itoh S. Eur J Org Chem 2004;14:3074–9.
[58] Mavinakuli P, Wei S, Wang Q, Karki AB, Dhage S, Wang Z, et al. J Phys Chem C 2010;114:3874–82.
[59] Mahmoudi M, Simchi A, Imani M, Milani AS, Stroeve P. J Phys Chem B 2008;112:14470–81.
[60] Zhang J, Chen J, Wang Z. Mater Lett 2007;61:1629–32.
[61] Sun J, Zhou S, Hou P, Yang Y, Weng J, Li X, et al. J Biomed Mater Res Part A 2007;80A:333–41.
[62] Deng J, Ding X, Zhang W, Peng Y, Wang J, Long X, et al. Polymer 2002;43:2179–84.
[63] Wang X, Tang S, Liu J, He Z, An L, Zhang C, et al. J Nanopart Res 2009;11:923–9.
[64] Yang C, Li H, Xiong D, Cao Z. React Funct Polym 2009;69:137–44.
[65] Qiu G, Wang Q, Nie M. J Appl Polym Sci 2006;102:2107–11.
[66] Feng X, Mao C, Yang G, Hou W, Zhu J. Langmuir 2006;22:4384–9.
[67] Trchová M, Konyushenko EN, Stejskal J, Kovárová J, Ciric-Marjanovic G. Polym Degrad Stab 2009;94:929–38.
[68] Liu YD, Park BJ, Kim YH, Choi HJ. J Mater Chem; 2011. doi:10.1039/C1JM12443A.
[69] Che RC, Peng LM, Duan XF, Chen Q, Liang XL. Adv Mater 2004;16(5):401–5.
[70] Grimes CA, Dickey EC, Mungle C, Ong KG, Qian D. J Appl Phys 2001;90:4134–7.
[71] Prigodin VN, Epstein AJ. Synth Met 2002;125:43–53.
[72] Wang ZH, Li C, Scherr EM, MacDiarmid AG, Epstein AJ. Phys Rev Lett 1991;66:1745–8.
[73] Haldar I, Biswas M, Nayak A. Synth Met 2011;161:1400–7.
[74] Joo J, Oh EJ, Min G, MacDiarmid AG, Epstein AJ. Synth Met 1995;69:251–4.
[75] Ray DK, Himanshu AK, Sinha TP. Indian J Pure Appl Phys 2007;45:692–9.
[76] Liu CD, Lee SN, Ho CH, Han JL, Hsieh K. J Phys Chem C 2008;112:15956–60.
[77] Sproul AB, Green MA. J Appl Phys 1991;70:846–54.
[78] Sudha JD, Pich A, Reena VL, Sivakala S, Adler HJP. J Mater Chem; 2011. doi:10.1039/C1JM13494A.
[79] Huang K, Qiu H, Wan M. Macromolecules 2002;35:8653–5.
[80] Lee K, Cho S, Park SH, Heeger AJ, Lee CW, Lee SH. Nature 2006;44:65–8.
[81] Joung EY, Tracy LB, Jung S, Loo Y. J Mater Chem 2008;18:3129–35.
[82] Marquardt P, Nimtz G, Mühlschlegel B. Solid State Commun 1988;65:539–42.
[83] Guo Z, Shin K, Karki A, Young D, Kaner R, Hahn H. J Nanopart Res 2009;11:1441–52.
[84] Gangopadhyay R, De A, Das S. J Appl Phys 2000;87:2363–71.
[85] Kryszewski M, Jeszka JK. Synth Met 1998;94:99–104.
[86] Xuan S, Hao L, Jiang W, Gong X, Hu Y, Chen Z. J Magn Magn Mater 2007;308:210–3.
[87] Zhang D, Karki AB, Rutman D, Young DP, Wang A, Cocke D, et al. Polymer 2009;50:4189–98.
[88] Hu P, Zhang S, Wang H, Pan D, Tian J, Tang Z, et al. J Alloys Compd 2011;509:2316–9.
[89] Niranjan MK, Velev JP, Duan CG, Jaswal SS, Tsymbal EY. Phys Rev B 2008;78:104405.
[90] Yoo JW, Jang HW, Prigodin VN, Kao C, Eom CB, Epstein AJ. Phys Rev B 2009;80:205207.
[91] Prigodin VN, Bergeson JD, Lincoln DM, Epstein AJ. Synth Met 2006;156:757–61.
[92] Mermer Ö, Veeraraghavan G, Francis TL, Sheng Y, Nguyen DT, Wohlgenannt M, et al. Phys Rev B 2005;72:205202.
[93] Parmenter RH, Ruppel W. J Appl Phys 1959;30:1548–58.